

Research Article

Quantitative analysis of yeast internal architecture using soft X-ray tomography

Maho Uchida¹, Yidi Sun², Gerry McDermott¹, Christian Knoechel¹, Mark A. Le Gros³, Dilworth Parkinson¹, David G. Drubin² and Carolyn A. Larabell^{1,3*}

¹Department of Anatomy, University of California at San Francisco, CA, USA

²Department of Molecular and Cell Biology, University of California at Berkeley, CA, USA

³Physical Biosciences Division, Lawrence Berkeley National Laboratory, CA, USA

*Correspondence to:

Carolyn A. Larabell, Box 2722
1550 4th St., University of
California at San Francisco, San
Francisco, CA 94143-2722.

E-mail:

Carolyn.Larabell@ucsf.edu

Abstract

We used soft X-ray tomography (SXT) — a high-resolution, quantitative imaging technique — to measure cell size and organelle volumes in yeasts. Cell size is a key factor in initiating cell division in yeasts, whereas the number and volume of the organelles have a profound impact on the function and viability of a cell. Consequently, determining these cell parameters is fundamentally important in understanding yeast biology. SXT is well suited to this type of analysis. Specimens are imaged in a near-native state, and relatively large numbers of cells can be readily analysed. In this study, we characterized haploid and diploid strains of *Saccharomyces cerevisiae* at each of the key stages in the cell cycle and determined the relationships that exist cellular and organelle volumes. We then compared these results with SXT data obtained from *Schizosaccharomyces pombe*, the three main phenotypes displayed by the opportunistic yeast pathogen *Candida albicans* and from a *coff1-22* mutant strain of *S. cerevisiae*. This comparison revealed that volumetric ratios were invariant, irrespective of yeast strain, ploidy or morphology, leading to the conclusion these volumetric ratios are common in all yeasts. Copyright © 2010 John Wiley & Sons, Ltd.

Keywords: imaging; cell cycle; organelles; karyoplasmic

Received: 16 August 2010
Accepted: 9 November 2010

Introduction

Cell size is a critical parameter in the regulation of cell division in yeasts (Bryan *et al.*, 2010; Conlon *et al.*, 2001; Johnston *et al.*, 1977; Jorgensen and Tyers, 2004; Umen, 2005). It has long been accepted that yeast cells must reach a minimum size before the process of cell division is initiated, and that the cells continue to grow as the cycle proceeds (Calvert and Dawes, 1984; Goranov *et al.*, 2009; Mitchison, 1957). As with all eukaryotes, yeast cells are compartmentalized into functionally distinct spaces by the creation of membrane-bound organelles. This subcellular arrangement maximizes both the complexity and the diversity of biochemical processes that can take place inside the

cell (Fagarasanu *et al.*, 2007; Warren and Wickner, 1996). During the cell cycle, organelle size must be precisely controlled for both proper cellular function and correct organelle partitioning between mother and daughter prior to their separation, since most organelles are inherited (Fagarasanu *et al.*, 2007; Warren and Wickner, 1996).

In the past it has been challenging to accurately measure the volume and density of organelles (Bryan *et al.*, 2010). Electron microscopy can only be used to image specimens that are less than 500 nm thick (Baumeister *et al.*, 1999). Consequently, even relatively small eukaryotic cells, such as yeasts, must be cut into sections 60–400 nm thick before they can be imaged. This requirement

makes imaging all organelles in a eukaryotic cell technically challenging and very time consuming (Leis *et al.*, 2009). Fluorescence microscopy has also been widely applied to imaging organelles (Giepmans *et al.*, 2006; Tsien, 2005). However, this technique can only provide data on organelles that have been fluorescently stained, and only a small number of organelles can be stained before overlap occurs between the emission/excitation bands of different coloured fluorescent probes. Moreover, in most cases it is difficult to accurately measure the actual volume of a labelled organelle, based on its fluorescence emission signal. In particular, it is very difficult to determine the volume of irregularly shaped organelles (such as lipid bodies, mitochondria and vacuoles) using fluorescence. Over the past decade, soft X-ray tomography (SXT) has emerged as a technique that is ideally suited to imaging and accurately quantifying organelle volumes (Gu *et al.*, 2007; Larabell and Le Gros, 2004a, 2004b; Le Gros *et al.*, 2005; Leis *et al.*, 2009; McDermott *et al.*, 2009; Parkinson *et al.*, 2008; Schneider *et al.*, 2002, 2003; Weiss *et al.*, 2000).

SXT has a number of highly advantageous characteristics in the context of imaging eukaryotic cells (McDermott *et al.*, 2009). First, the short wavelength of the illuminating X-rays allows specimens to be imaged at high spatial resolution (Kirz *et al.*, 1995; Larabell and Le Gros, 2004a; McDermott *et al.*, 2009; Weiss *et al.*, 2000, 2001). Second, soft X-ray photons can penetrate and image fully hydrated specimens up to 15 μm thick (Attwood, 1999; Kirz *et al.*, 1995; Le Gros *et al.*, 2005; Schneider, 2003). Lastly, image contrast is obtained directly from the absorption of soft X-rays by the specimen, and therefore no potentially damaging specimen staining procedures are required (Le Gros *et al.*, 2005; McDermott *et al.*, 2009). In SXT the specimen-illuminating photons are in a region of the electromagnetic spectrum known as the 'water window'. This lies between the K shell absorption edges of carbon (284 eV, $\lambda = 4.4$ nm) and oxygen (543 eV, $\lambda = 2.3$ nm) (Attwood, 1999; Kirz *et al.*, 1995; Le Gros *et al.*, 2005; McDermott *et al.*, 2009; Schmahl *et al.*, 1996; Weiss *et al.*, 2001). X-ray photons within this energy range are absorbed an order of magnitude more strongly by carbon- and nitrogen-containing biomolecules than by water (Le Gros *et al.*, 2005). This absorption adheres to Beer-Lambert's law and is therefore linear with thickness (Attwood, 1999;

Uchida *et al.*, 2009). Consequently, images produced by SXT are quantitative, with each biochemical component having a specific X-ray linear absorption coefficient (LAC) (Le Gros *et al.*, 2005; Weiss and 2000). Therefore, organelles and other cell structures can be visualized directly, based on differences in biochemical composition and density. For example, dense lipid-rich structures absorb soft X-rays much more strongly than organelles with relatively high water content, for example vacuoles. This contrast mechanism is highly sensitive to subtle changes in LAC, e.g. the nucleolus can be very readily identified in a reconstruction of a yeast nucleus (Uchida *et al.*, 2009).

As with all tomographic imaging techniques, in SXT a number of projection images are collected and then used to calculate a volumetric reconstruction of the specimen (Leis *et al.*, 2009; McDermott *et al.*, 2009). In this work, projection images were collected using XM-2, a soft X-ray microscope dedicated to biological and biomedical imaging. The spatial resolution in images produced by XM-2 is determined by the zone plate optics (Attwood, 1999; Le Gros *et al.*, 2005; McDermott *et al.*, 2009). For all of the specimens imaged in this work the spatial resolution was 50 nm. In the near future, incorporation of the latest generation of zone plates into XM-2 will increase the achievable spatial resolution to better than 20 nm (Chao *et al.*, 2005).

Yeasts have been a workhorse model eukaryotic cell for many years, particularly for studying cell division and the effects of engineered mutations. Recently, much work has been carried out on determining the genetic and molecular mechanisms of organelle inheritance in the budding yeast *Saccharomyces cerevisiae* (Umen, 2005; Zimmerberg and Kozlov, 2006). It is now generally accepted that the actin cytoskeleton and associated motors orchestrate organelle localization during cell division. However, details of the mechanisms that regulate organelle size in yeast during the cell cycle remain unclear in general, the exception being regulation of nuclear size, where there has been significant progress to date (Jorgensen *et al.*, 2007; Neumann and Nurse, 2007). In both budding and fission yeast the growth of the nucleus has been shown to be proportional to cell size (Jorgensen *et al.*, 2007; Neumann and Nurse, 2007). It has also been well established that ploidy has a direct bearing on cell size (Murray *et al.*, 1987). Therefore, in this study

we imaged both haploid and diploid strains of *S. cerevisiae* to determine the effects of ploidy and cell cycle on the size of the cells and organelles. We observed ratios existing between cell size and organelle volumes were conserved, irrespective of ploidy or stage in the cell cycle. We then compared data obtained from *S. cerevisiae* with that from other strains of yeasts, including a strain of *Candida albicans* that undergoes phenotypic switching (Uchida *et al.*, 2009). In this way we examined these volumetric ratios in specimens across a range of yeast cell types and morphologies.

Materials and methods

Strains, cell cultures, and growth conditions

Diploid (DDY1102), haploid (DDY904) and *coff1-22* mutant (DDY1266) of *S. cerevisiae* strains were grown at 25 °C to early log phase in YPD medium. *S. cerevisiae* (diploid, ATCC 200 060) was grown at 30 °C to early log phase in YEPD medium. *C. albicans* (ATCC 26555) was grown in YM medium at 26 °C for the formation of yeast-like cells, at 30 °C for formation of germ tubes and at 37 °C for hyphal form. *Sz. pombe* (strain no. 972h) was grown at 30 °C to early log phase in YES medium. All media were supplemented with the appropriate amino acids.

Soft X-ray tomography

Projection images were collected using XM-2, the National Center for X-ray Tomography soft X-ray microscope at the Advanced Light Source of Lawrence Berkeley National Laboratory. XM-2 was designed to image biological samples in their hydrated states. Specimens were simply transferred from the growth chamber, mounted in thin-walled glass capillary tubes and rapidly cryo-immobilized prior to being mounted in the cryogenic specimen rotation stage on the microscope (Le Gros *et al.*, 2005). During data collection, the cells were maintained in a stream of helium gas that had been cooled to liquid nitrogen temperatures (Le Gros *et al.*, 2005; McDermott *et al.*, 2009). Cooling the specimen allows collection of projection images while mitigating the effects of exposure to radiation. Each dataset (i.e. 90 projection images spanning a range of 180°) was collected using a Fresnel zone plate-based objective lens with a resolution

of 50 nm (Larabell and Le Gros, 2004a). Exposure times for each projection image was in the range 150–300 ms. Projection images were manually aligned using IMOD software by tracking fiducial markers on adjacent images (Kremer *et al.*, 1996). Tomographic reconstructions were calculated using the iterative reconstruction method (Mastronarde, 2005; Stayman and Fessler, 2004). The Amira software package (Mercury Computer Systems) was used to manually segment the reconstructed volumes, measure voxel values (i.e. absorption values in volume element of the reconstructed data) to calculate linear absorption coefficients (LACs) and create the movies included in the supporting information.

Results

In the first instance we quantified the change in cell and organelle volumes during the cell cycle in *S. cerevisiae* using soft X-ray tomography. These measurements were done for both haploid and diploid cells without preselecting cells at a certain stage of the cell cycle, e.g. techniques such as fluorescence activated cell sorting (FACS), centrifugal elutriation, or chemically/biochemically inducing cell cycle arrest. Cells undergoing log phase growth (OD = 0.1–0.4) were mounted in glass capillary tubes and immediately cryo-immobilized; therefore, cells were imaged with minimal perturbation from their native growth conditions. It has been well established from electron microscopy/tomographic imaging that use of chemical fixation agents leads to significant damage to cellular structures. In total we collected approximately 80 tomographic datasets. Since each field of view in the soft X-ray microscope used for this work is approximately 15 × 15 μm, between one and six yeast cells were imaged per dataset and, as a result, more than 200 cells were analysed in total.

Once the projection images were reconstructed, the volumes were segmented to isolate individual cells and subsequently their component organelles (Figure 1A). The reconstructed cells were segmented into discrete volumes based on the LACs (Figure 1B). For instance, volumes assigned as dense lipid bodies have an average LAC value of 0.55 μm⁻¹ compared with more transmissive organelles, such as nuclei, nucleoli, vacuoles and mitochondria, that have typical LAC values of 0.26,

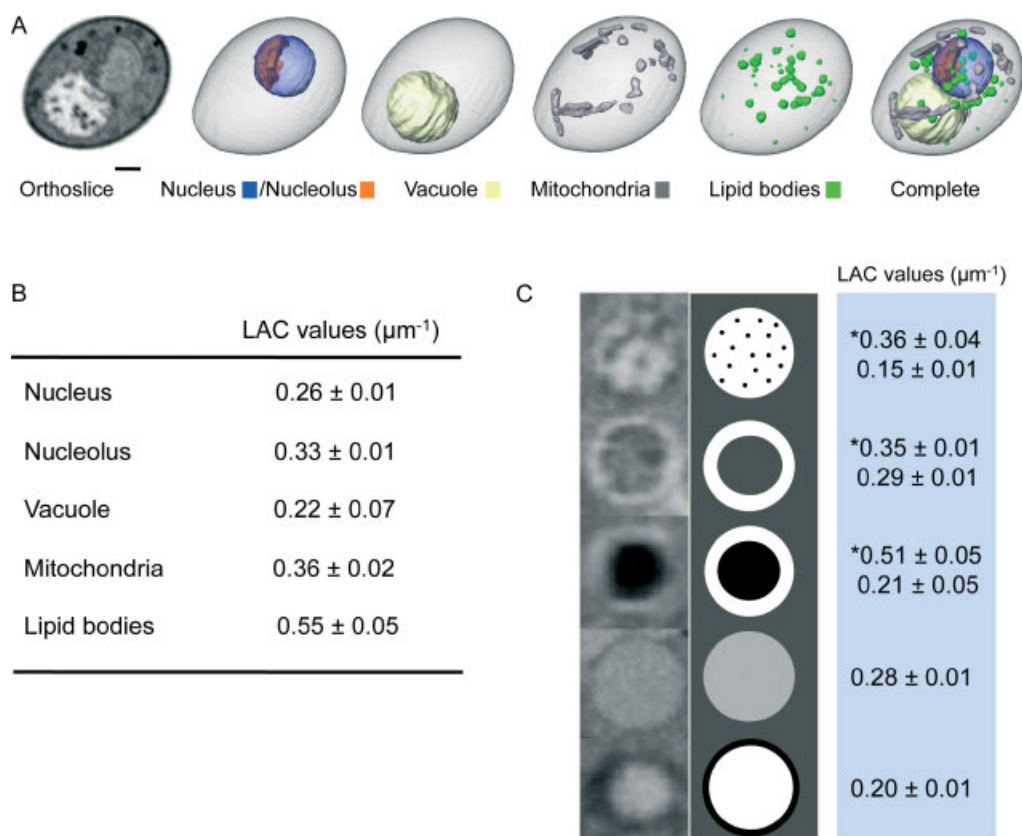


Figure 1. Segmentation of organelles based on linear absorption coefficient (LAC) values. (A) A representative diploid cell shown in an orthoslice (i.e. a single slice of tomographic data) and individually segmented organelles; scale bar = 1 μm . (B) LAC values for each organelles. (C) Five different vacuolar compositions found in tomographic data [left; the similar sizes of vacuoles were selected (i.e., $\sim 1 \mu\text{m}$)], schematic views (middle) and LAC values (right; *indicates LAC values of structures inside vacuoles)

0.33, 0.22 and $0.36 \mu\text{m}^{-1}$, respectively. Assignment of organelle type to a particular segmented volume was guided by morphological characteristics established by other modalities. For example, the nuclei/nucleoli, mitochondria and vacuoles have distinct and very recognizable morphologies. Once vacuoles from a number of cells had been segmented, it was clear that they could be categorized into one of five types, based on their morphology, internal structure and densities. The LAC values for these are shown in Figure 1C.

Representative cells from each stage of the cell cycle are shown in Figure 2A. All the segmented cells were categorized into the appropriate phase of the cell cycle, based on the morphological state of cells and their organelles. It was assumed that these cells were actively going through the cell cycle until the instant they were

cryo-immobilized. Using these segmented cells, we quantified cell (Figure 2B), cytosol (Figure 2C) and organelle (Figure 3) volumes, together with their surface areas (Figure 4). In haploid cells, the cell volumes were within the range $10\text{--}50 \mu\text{m}^3$ in G_1 , $20\text{--}60 \mu\text{m}^3$ in S, $40\text{--}80 \mu\text{m}^3$ in G_2 and $60\text{--}100 \mu\text{m}^3$ in M phase. In diploid cells, the cell volumes were within $20\text{--}60 \mu\text{m}^3$ in G_1 , within $30\text{--}80 \mu\text{m}^3$ in S, within $50\text{--}140 \mu\text{m}^3$ in G_2 and within $70\text{--}140 \mu\text{m}^3$ in M phase. The minimum size requirement to be in G_1 phase was observed to be $10 \mu\text{m}^3$ in haploid and $20 \mu\text{m}^3$ in diploid cells. A similar trend of cell volume distribution was also observed in diploid cells of another *S. cerevisiae* strain (ATCC200060; see supporting information, Figure S1). The average cytosolic volume (Figure 2C) was calculated by combining the cell wall/membrane volume with the total volume

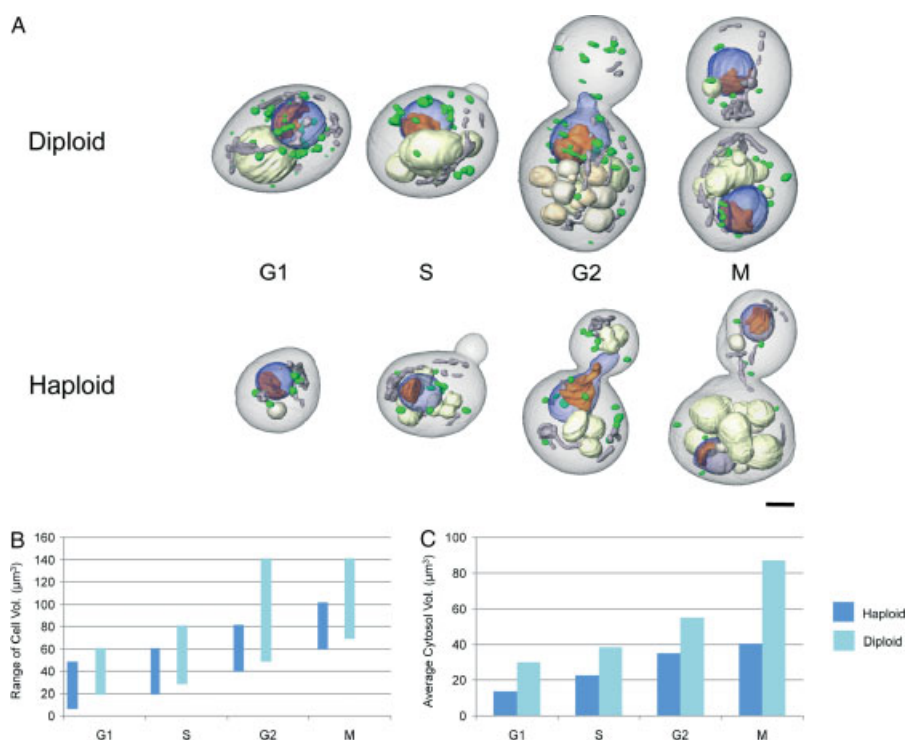


Figure 2. Measurement of cell volumes using segmented cells. (A) Representative haploid and diploid *S. cerevisiae* cells at the four main stages of the cell cycle; scale bar = 1 µm. (B) Comparison of cell volumes in diploid and haploid cells. For this measurement, a total of 74 haploid cells and 80 diploid cells were analysed. (C) Average cytosolic volume in diploid and haploid cells

of segmented organelles and then subtracting this combined volume from the total cell volume. On average, the nucleus occupied 6–11% of cell volume; the nucleolus occupied 20% of the nucleus; vacuole(s) occupied 3–14% of the cell; and mitochondria and lipid bodies occupied 1–2% of the cell (Figure 3); therefore, the cytosol, other non-segmented organelles, large macromolecular complexes, such as the ribosomes, and the cytoskeleton occupy the remaining 70% of cell volume. The overall trend observed in the surface area of lipid bodies, mitochondria, vacuoles and nucleus mirrored that of the organelle volumes (Figure 4).

We next examined how the major organelle volume correlates with the cell size as the cell cycle progresses (Figure 5A). In haploid cells, the ratio of total major organelle volume to cell volume (O:C ratio) was relatively constant through out the cell cycle (i.e. G₁, 0.17; S, 0.18; G₂, 0.18; M, 0.16). In diploid cells, the O:C ratio dropped slightly at M phase (i.e. 0.16) compared to the O:C ratios during G₁ through G₂ (i.e. G₁, 0.22; S, 0.24;

G₂, 0.20); however, overall it appears that there is a linear correlation between cell size and major organelle volume in both haploid and diploid cells.

To determine whether the O:C ratio is consistent for each organelle, we obtained the O:C ratio for lipid bodies, mitochondria, vacuoles (Figure 5B, C) and nucleus (Figure 5D). Interestingly, the O:C ratio for lipid bodies and mitochondria (i.e. ~0.01) was constant throughout the cell cycle in both diploid and haploid cells. The O:C ratio for vacuoles was, however, much larger compared to those of lipid bodies and mitochondria. In haploid cells, the O:C ratio for vacuoles increased as the cell cycle proceeded (i.e. G₁, 0.04; S, 0.06; G₂, 0.07; M, 0.13). In contrast with the haploid cells, the O:C ratio for vacuoles in diploid cells showed a slight increase in ratio from G₁ (0.09) to S (0.11) and then declined from S (0.11) to G₂ (0.09) and M (0.05). Similar to the O:C ratio for lipid bodies and mitochondria, the O:C ratio for the nucleus was fairly constant throughout the cell cycle in both haploid and diploid cells (i.e. 0.07–0.09).

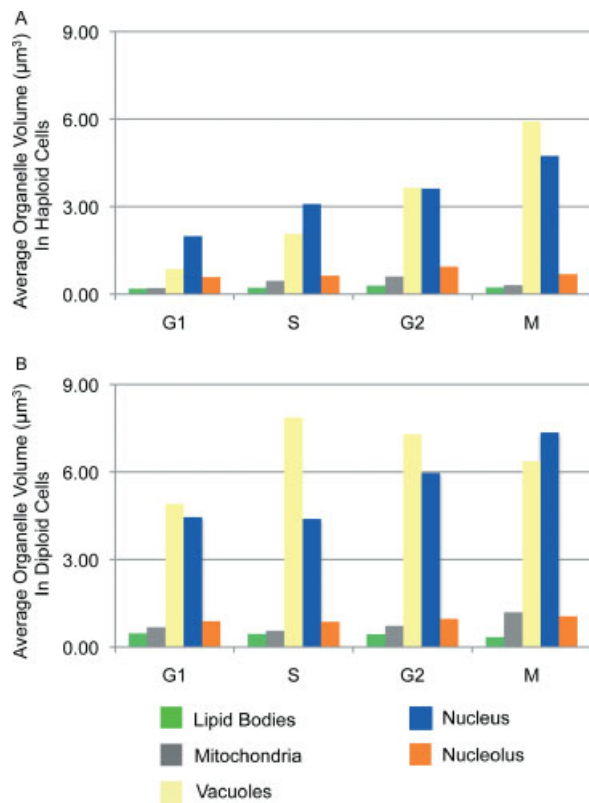


Figure 3. Average volume of organelles in haploid (A) and diploid (B) cells

This result was similar to the ratio of nuclear to cell volume previously reported for both budding and fission yeast (Jorgensen *et al.*, 2007; Neumann and Nurse, 2007), in that the growth of nucleus was consistently proportional with cell growth. We also observed that all organelles, except vacuoles, grew in direct proportion to cell size. Therefore, we conclude that the slight variation seen in the ratio of total organelle volume to cell volume (Figure 5A) was mainly due to the volume of vacuoles.

We quantified the ratio of nucleolus to nuclear volume (N:Nuc ratio; Figure 5E). Similar to the ratio of nuclear to cell volumes, the N:Nuc ratio was relatively similar between haploid (0.14–0.26) and diploid (0.17–0.21) cells. In haploid cells, the N:Nuc ratio in G₁, S and G₂ was, however, higher than those of diploid cells, indicating that the nucleolus in these stages of haploid cells was slightly larger relative to the size of nucleus.

To better understand cell size control and organelle inheritance during bud emergence and formation of the daughter cell, we measured cell

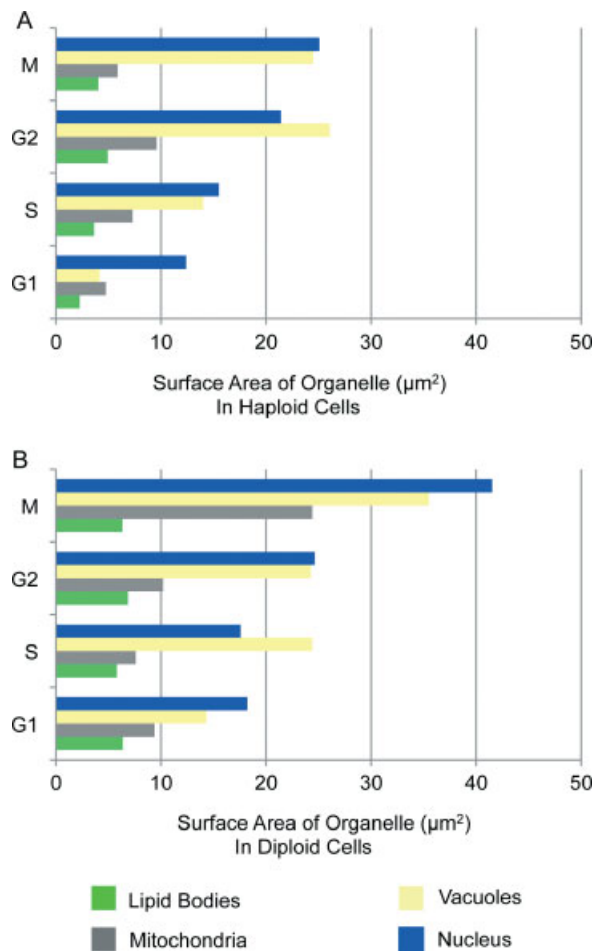


Figure 4. Average surface area of organelles in haploid (A) and diploid (B) cells

and organelle volumes in daughter and mother cells separately. The bud scar(s) on the cell surface was readily identified (an example of bud scars is shown in the supporting information, Figure S2). In this study, about 67% of cells had no bud scar, 14% of cells had one bud scar, 12% of cells had two bud scars, and <6% of cells had three to seven bud scars. As shown in Figure 6A, there was a linear increase in the ratio of daughter to mother cell volume (D:M ratio) in both haploid and diploid cells, indicating that the size of both increases as the cell cycle progresses. In haploid cells, the D:M ratio of G₂ was approximately 1.3 times larger (G₂, 0.37) than those of diploid cells (G₂, 0.29). We then compared the ratio of total organelle volume to cell volume (O:C ratio) in daughter and mother cells (Figure 6B). In haploid cells, the O:C ratio for

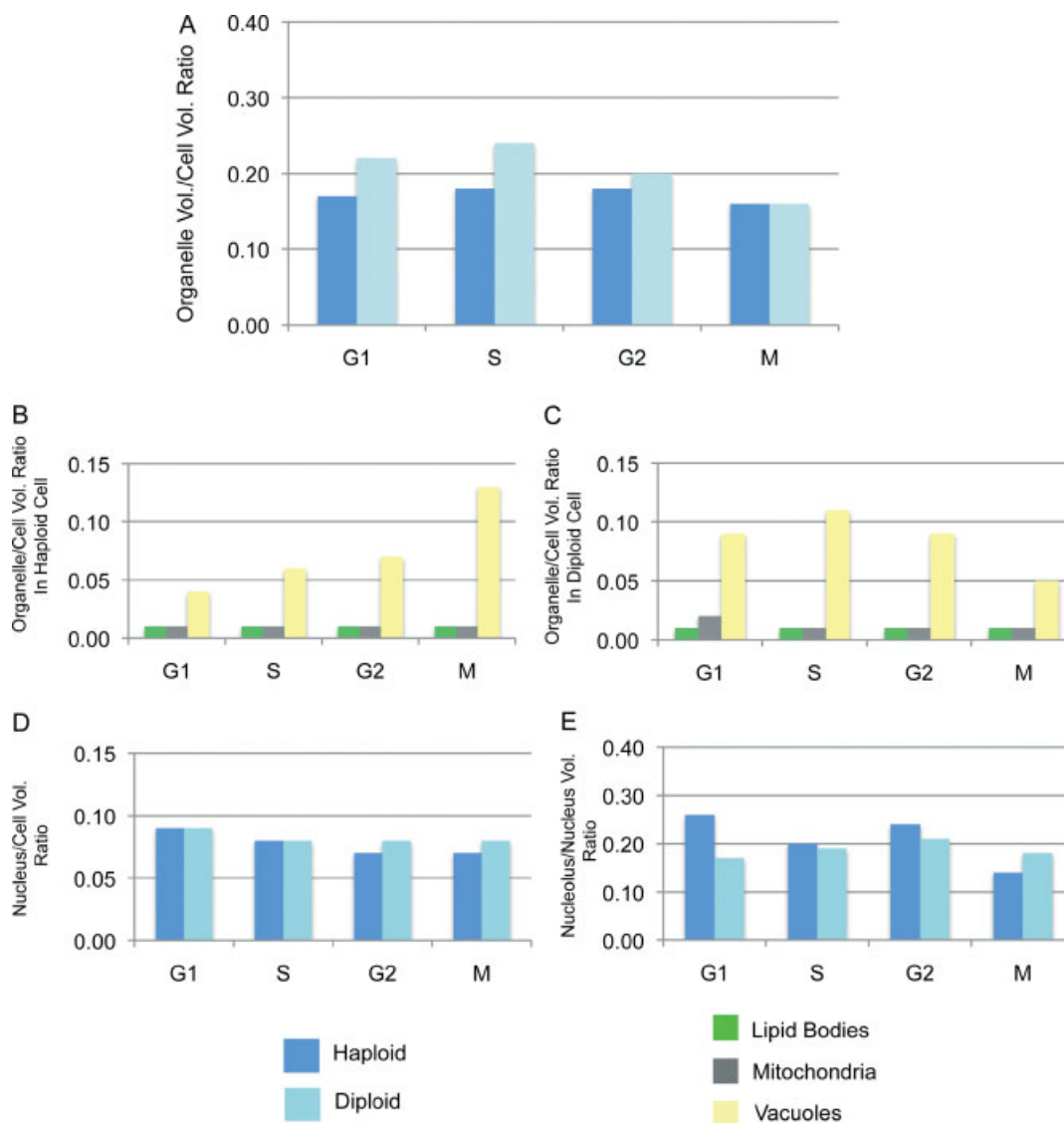


Figure 5. Analysis of organelle and cell size linkage during cell cycle. (A) The ratio of total organelle volume to cell volume (O:C ratio) in haploid and diploid cells. (B) The O:C ratio for lipid bodies, mitochondria and vacuoles in haploid cells. (C) The O:C ratio for lipid bodies, mitochondria and vacuoles in diploid cells. (D) The O:C ratio for nucleus in haploid and diploid cells. (E) The ratio of nucleolus volume to nucleus volume in haploid and diploid cells

mother cells was similar in S (0.17) and G₂ (0.18), but the O:C ratio was increased by ~1.5-fold in M (0.28). In contrast, the O:C ratio for daughter cells was similar in G₂ (0.11) and M (0.10) but decreased 10-fold in S (0.01). In diploid cells, the O:C ratio for mother cells was identical in S (0.22) and G₂ (0.22) but was decreased by 1.4-fold in M (0.16), whereas the O:C ratio for daughter cells was identical in S (0.01) and G₂ (0.01) but increased by 11-fold in M (0.11). Overall, the

O:C ratios in daughter and mother cells were not as constant as those in the whole cells. In addition, it appears that the timing of organelle partitioning from the mother to the daughter cells was different in haploid and diploid cells.

This work demonstrates that both haploid and diploid cells of *S. cerevisiae* maintain a constant ratio of total major organelle volume to cell volume throughout the cell cycle. To find out whether this correlation was influenced by morphology,

species or mutation, we characterized *C. albicans*, *Sz. pombe* and a *S. cerevisiae* mutant. Surprisingly, similar O:C ratios (i.e. 0.18–0.21) were observed in *C. albicans* that exhibited three different phenotypes (i.e. yeast-like, germ tubes and hyphae), *Sz. pombe* cells at the different stages of cell cycle, and cofilin mutant cells (*coff1-22*) (data not shown). The ratio of nuclear to cell volume was also similar among all of these different yeasts (i.e. 0.05–0.08). Therefore, it appears that maintaining the ratio of organelle volume to cell volume is important for the cells to grow and divide, and that these ratios are common over a wide range of yeast strains and morphologies.

In this study, vacuoles were observed to have different compositions (Figure 1C). These were verified by the linear absorption coefficient (LAC) values and categorized into five types. The type A vacuole had numerous small, dense inclusions. The type B and C vacuoles were similar to each other, in that both appeared to have a dense region that occupied the majority of the vacuole core; however, this portion was much more highly absorbing in type C vacuoles. The type D and E vacuoles were also similar to each other, but quite different from the type A–C vacuoles. Types D and E did not contain any inclusions or dense regions, but appeared to be mostly aqueous, although the type D vacuole had a slightly higher LAC value compared to that of the type E. Although we did not observe any strong correlation between the vacuole content morphology and its location in the cell or stage of the cell cycle, it seems likely that these patterns represent different functional processes (examples of their relative location in the cell are shown in the supporting information, Figure S3). It is known that vacuoles participate in various processes, such as protein degradation, metabolic storage, ion homeostasis and osmoregulation (Klionsky *et al.*, 1990), as do their counterpart in mammalian cells, lysosomes, and vacuoles in plant cells (Gieselmann and Braulke, 2009). In future work it will be important to determine the functional consequences of these differences in vacuolar composition.

Discussion

Cell size and organelle volumes are enormously important physical characteristics that must be

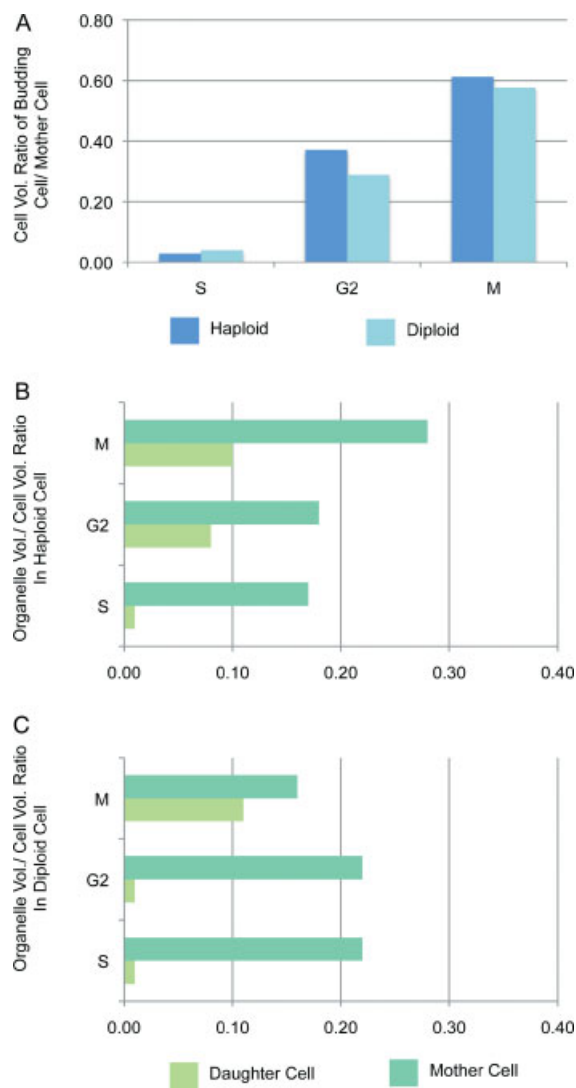


Figure 6. Analysis of organelle and cell size linkage in mother and daughter cells. (A) The ratio of budding: daughter cell volume to mother cell volume in haploid and diploid cells. The O:C ratio in haploid (B) and diploid (C) cells

monitored and controlled in response to changing environmental conditions, phenotype and the cell cycle. Soft X-ray tomography allows the internal architecture of cells in a near-native state to be imaged and quantified with high spatial resolution. The images produced by this technique have excellent natural contrast without requiring the cells to be first stained or dehydrated. Moreover, compared to other high-resolution tomographic imaging techniques, SXT is capable of

high-throughput imaging. Since each reconstruction typically contains three to five yeast cells, this allows analysis of significant numbers of cells; for example, in this work more than 200 cells were reconstructed.

In this study we focused primarily on measuring cell size and the volumes of the major organelles in haploid and diploid strains of *S. cerevisiae* at the four key stages of the yeast cell cycle. We determined that the growth of the major organelles — with the notable exception of vacuoles — is strictly regulated in accordance with cell size. We observed the relative ratio of organelle to cell volumes to remain constant throughout the cell cycle. We also determined that the ratio of nucleolus to nuclear volume and ratio of nuclear to cell volumes were similar at all stages of the cell cycle. We expanded this study to include an examination of these ratios in *Sz. pombe* and *C. albicans* and found similar ratios to be maintained. Therefore, we conclude that in yeasts there are well-defined optimal volumetric ratios and, since these were observed to be independent of strain, ploidy and phenotype, that these ratios are likely to be common to all yeast cells. We plan to extend this analysis in the future, with the goal of using mutant cells to improve our understanding of how cells control their size and that of their component organelles.

Acknowledgements

We gratefully acknowledge Zenny Serrano for cell culture and expert technical assistance. This work was funded by the Department of Energy Office of Biological and Environmental Research Grant DE-AC02-05CH11231, the NIH National Center for Research Resources Grant RR019664 and NIH R01 50399 to DGD.

Supporting information on the internet

The following supporting information may be found in the online version of this article:

Movie S1. A movie of the representative diploid and haploid cells from each phase of cell cycle

Figure S1. Comparison of cell volumes in two strains of diploid cells, ATCC200060 and DDY1102

Figure S2. Bud scars on the surface of the mother cells shown within the bounded areas

Figure S3. Representative cells shown in orthoslice, demonstrating the relative locations of vacuoles and their different components in the cell

References

- Attwood DT. 1999. *Soft X-rays and Extreme Ultraviolet Radiation: Principles and Applications*. Cambridge University Press: Cambridge.
- Baumeister W, Grimm R, Walz J. 1999. Electron tomography of molecules and cells. *Trends Cell Biol* **9**: 81–85.
- Bryan AK, Goranov A, Amon A, Manalis SR. 2010. Measurement of mass, density, and volume during the cell cycle of yeast. *Proc Natl Acad Sci USA* **107**: 999–1004.
- Calvert GR, Dawes IW. 1984. Cell-size control of development in *Saccharomyces cerevisiae*. *Nature* **312**: 61–63.
- Chao WL, Harteneck BD, Liddle JA, *et al.* 2005. Soft X-ray microscopy at a spatial resolution better than 15 nm. *Nature* **435**: 1210–1213.
- Conlon IJ, Dunn GA, Mudge AW, Raff MC. 2001. Extracellular control of cell size. *Nat Cell Biol* **3**: 918–921.
- Fagarasanu A, Fagarasanu M, Rachubinski RA. 2007. Maintaining peroxisome populations: a story of division and inheritance. *Annu Rev Cell Dev Biol* **23**: 321–344.
- Giepmans BNG, Adams SR, Ellisman MH, *et al.* 2006. The fluorescent toolbox for assessing protein location and function. *Science* **312**: 217–224.
- Gieselmann V, Braulke T. 2009. Lysosomes preface. *Biochim Biophys Acta Mol Cell Res* **1793**: 603–604.
- Goranov AI, Cook M, Rivicova M, *et al.* 2009. The rate of cell growth is governed by cell cycle stage. *Genes Dev* **23**: 1408–1422.
- Gu WW, Etkin LD, Le Gros MA, Larabell CA. 2007. X-ray tomography of *Schizosaccharomyces pombe*. *Differentiation* **75**: 529–535.
- Johnston GC, Pringle JR, Hartwell LH. 1977. Coordination of growth with cell division in the yeast *Saccharomyces cerevisiae*. *Exp Cell Res* **105**: 79–98.
- Jorgensen P, Edgington NP, Schneider BL, *et al.* 2007. The size of the nucleus increases as yeast cells grow. *Mol Biol Cell* **18**: 3523–3532.
- Jorgensen P, Tyers M. 2004. How cells coordinate growth and division. *Curr Biol* **14**: R1014–1027.
- Kirz J, Jacobsen C, Howells M. 1995. Soft X-ray microscopes and their biological applications. *Q Rev Biophys* **28**: 33–130.
- Klionsky DJ, Herman PK, Emr SD. 1990. The fungal vacuole: composition, function, and biogenesis. *Microbiol Rev* **54**: 266–292.
- Kremer JR, Mastrorade DN, McIntosh JR. 1996. Computer visualization of three-dimensional image data using IMOD. *J Struct Biol* **116**: 71–76.
- Larabell C, Le Gros M. 2004a. Whole cell cryo X-ray tomography and protein localization at 50 μm resolution. *Biophys J* **86**: 185A.
- Larabell CA, Le Gros MA. 2004b. X-ray tomography generates 3D reconstructions of the yeast *Saccharomyces cerevisiae* at 60 nm resolution. *Mol Biol Cell* **15**: 957–962.
- Le Gros MA, McDermott G, Larabell CA. 2005. X-ray tomography of whole cells. *Curr Opin Struct Biol* **15**: 593–600.

- Leis A, Rockel B, Andrees L, Baumeister W. 2009. Visualizing cells at the nanoscale. *Trends Biochem Sci* **34**: 60–70.
- Mastrorade DN. 2005. Fiducial marker and hybrid alignment methods for single- and double-axis tomography. In *Electron Tomography: Methods for Three-dimensional Visualization of Structures in the Cell*, Frank J (ed.). Springer: Berlin; 163–185.
- McDermott G, Le Gros MA, Knoechel CG, et al. 2009. Soft X-ray tomography and cryogenic light microscopy: the cool combination in cellular imaging. *Trends Cell Biol* **19**: 587–595.
- Mitchison JM. 1957. The growth of single cells. 1. *Schizosaccharomyces pombe*. *Exp Cell Res* **13**: 244–262.
- Murray LE, Veinotdrobot LM, Hanijoyce PJ, et al. 1987. Effect of ploidy on the critical size for cell proliferation of the yeast *Saccharomyces cerevisiae*. *Curr Genet* **11**: 591–594.
- Neumann FR, Nurse P. 2007. Nuclear size control in fission yeast. *J Cell Biol* **179**: 593–600.
- Parkinson DY, McDermott G, Etkin LD, et al. 2008. Quantitative 3D imaging of eukaryotic cells using soft X-ray tomography. *J Struct Biol* **162**: 380–386.
- Schmahl G, Rudolph D, Schneider G, et al. 1996. Diffraction optics for X-ray imaging. *Microelectron Eng* **32**: 351–367.
- Schneider G. 2003. X-ray microscopy: methods and perspectives. *Anal Bioanal Chem* **376**: 558–561.
- Schneider G, Anderson E, Vogt S, et al. 2002. Computed tomography of cryogenic cells. *Surface Rev Lett* **9**: 177–183.
- Schneider G, Denbeaux G, Anderson E, et al. 2003. High resolution X-ray tomography with applications in biology and materials science. *J Physique IV* **104**: 607–613.
- Stayman JW, Fessler JA. 2004. Compensation for nonuniform resolution using penalized-likelihood reconstruction in space-variant imaging systems. *IEEE Trans Med Imag* **23**: 269–284.
- Tsien RY. 2005. Building and breeding molecules to spy on cells and tumors. *FEBS Lett* **579**: 927–932.
- Uchida M, McDermott G, Wetzler M, et al. 2009. Soft X-ray tomography of phenotypic switching and the cellular response to antifungal peptoids in *Candida albicans*. *Proc Natl Acad Sci USA* **106**: 19375–19380.
- Umen JG. 2005. The elusive sizer. *Curr Opin Cell Biol* **17**: 435–441.
- Warren G, Wickner W. 1996. Organelle inheritance. *Cell* **84**: 395–400.
- Weiss D. 2000. Computed Tomography Based on Cryo-X-ray Microscopic Images of Unsectioned Biological Specimens. Cuvillier Verlag: Georg-August University of Göttingen (thesis, ISBN-13:9783897129702).
- Weiss D, Schneider G, Niemann B, et al. 2000. Computed tomography of cryogenic biological specimens based on X-ray microscopic images. *Ultramicroscopy* **84**: 185–197.
- Weiss D, Schneider G, Vogt S, et al. 2001. Tomographic imaging of biological specimens with the cryo-transmission X-ray microscope. *Nucl Instrum Methods Physics Res A* **467**: 1308–1311.
- Zimmerberg J, Kozlov MM. 2006. How proteins produce cellular membrane curvature. *Nat Rev Mol Cell Biol* **7**: 9–19.